ISBN: 978-3-95450-216-5 doi:10.18429/JACoW-eeFACT2018-TUPBB03

PERFORMANCE OF THE FCC-ee POLARIMETER

N. Y. Muchnoi*,
Budker Institute of Nuclear Physics, 630090 Novosibirsk, Russian Federation
also at the Novosibirsk State University, 630090 Novosibirsk, Russian Federation

Abstract

Inverse Compton scattering is the classical way to measure the electron beam polarization. Eligibility of the approach at high energy domain has been demonstrated by LEP [1,2], HERA [3] and SLD [4] experiments. Fast measurement of beam polarization allows to apply the resonant depolarization technique for precise beam energy determination [5,6]. The distinctive feature of the FCC-ee polarimeter is the registration of scattered electrons along with scattered photons. Polarimeter is designed to measure the transverse polarization of the non-colliding pilot bunch with 1% accuracy every second. Furthermore the same apparatus allows to measure the beam energy, longitudinal beam polarization (if any) and transverse beam positions/sizes at the place of installation.

INTRODUCTION

The illustration for the process of Inverse Compton Scattering (ICS) is presented in Fig. 1.

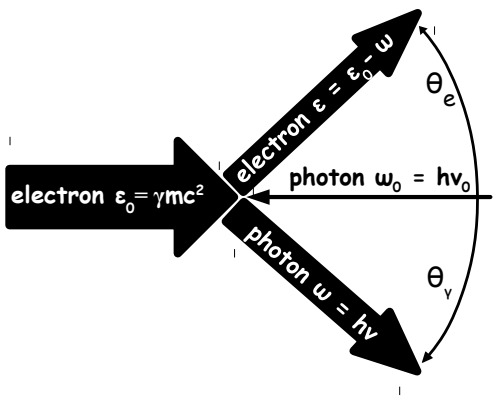

Figure 1: Inverse Compton scattering: the thickness of every arrow qualitatively reflects the energy of each particle. ω_0, ε_0 and ω, ε are the energies of the photon and electron in their initial and final states correspondingly, while θ_γ and θ_e are the scattering angles of photon and electron.

Considering an ultra-relativistic case ($\varepsilon_0, \varepsilon, \omega \gg \omega_0$) we introduce the universal scattering parameter

$$u = \frac{\omega}{\varepsilon} = \frac{\theta_e}{\theta_\gamma} = \frac{\omega}{\varepsilon_0 - \omega} = \frac{\varepsilon_0 - \varepsilon}{\varepsilon}, \qquad (1)$$

bearing in mind the energy and transverse momenta conservation laws while neglecting the corresponding impacts of initial photon. Parameter u lies within the range $u \in [0, \kappa]$ and is limited from above by the longitudinal momenta conservation: κ is twice the initial energy of the photon in the rest frame of the electron, expressed in units of the electron rest energy:

$$\kappa = 4\frac{\omega_0 \varepsilon_0}{(mc^2)^2} = 2 \times 2\gamma \frac{\omega_0}{mc^2}. \qquad (2)$$

If the electron-photon interaction is not head on, the angle of interaction $\alpha \neq \pi$ affects the initial photon energy seen by the electron, and κ parameter becomes[1]

$$\kappa(\alpha) = 4\frac{\omega_0 \varepsilon_0}{(mc^2)^2} \sin^2\left(\frac{\alpha}{2}\right). \qquad (3)$$

Almost any experimental application of the backscattering of laser radiation on the electron beam for any reason implies the use of the scheme shown in Fig. 2. Laser radiation is inserted into the machine vacuum chamber, directed and focused to the interaction point where scattering occurs. The dipole is used to separate scattered photons (and electrons) from the electron beam, propagating in the machine's vacuum chamber. x-axis and z-axis define the coordinate system in the interaction point, the plane of the figure is the plane of machine, the vertical y-axis is perpendicular to the plane of figure. After the dipole, the coordinate system (x', z') is rotated by the beam bending angle θ_0.

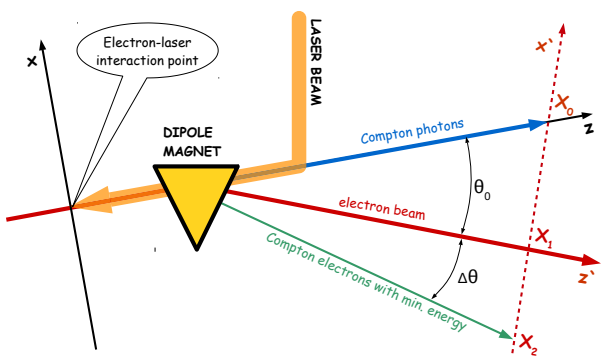

Figure 2: Regular layout of ICS experiments realization.

For the FCC-ee polarimeter we assume the interaction of laser radiation with electrons in the electron energy range $\varepsilon_0 \in [45 : 185]$ GeV. The energy of the laser photon ω_0 is coupled with the radiation wavelength in vacuum λ_0: $\omega_0 = hc/\lambda_0$, where hc =1.239 841 93 eV·μm. In particular when λ_0 =1 μm, ε_0 =100 GeV and $\alpha = \pi$ one obtains the "typical" value of κ parameter for the FCC-ee case, $\kappa \simeq 1.9$. Maximum energy of backscattered photon ω_{max} obviously

* N.Yu.Muchnoi@inp.nsk.su

[1] this is correct when $\tan(\alpha/2) \gg 1/\gamma$.

ISBN: 978-3-95450-216-5 doi:10.18429/JACoW-eeFACT2018-TUPBB03

corresponds to the minimal energy of scattered electron ε_{min}, both values are easily obtained from definitions Eq. (1) – Eq. (3) when $u = \kappa$:

$$\omega_{max} = \frac{\varepsilon_0 \kappa}{1+\kappa} \text{ and } \varepsilon_{min} = \frac{\varepsilon_0}{1+\kappa}. \tag{4}$$

Note that $\omega_{max} = \varepsilon_{min}$ when $\kappa = 1$. It's not hard to show that the scattering angles of photon θ_γ and electron θ_e (see Fig. 1) depend on u and κ as:

$$\theta_\gamma = \frac{1}{\gamma}\sqrt{\frac{\kappa}{u} - 1} \text{ and } \theta_e = \frac{u}{\gamma}\sqrt{\frac{\kappa}{u} - 1}. \tag{5}$$

The electron scattering angle θ_e can not exceed the limit $\max(\theta_e) = \kappa/2 \cdot \gamma = 2\omega_0/mc^2$ and we see that this value does not depend on ε_0.

ICS Cross Section

ICS cross section depends on polarization states of all initial and final particles [7]. It is common to average the polarization terms of the final states, then the cross section depends solely from the initial photon and electron polarizations. In order do describe polarization states of the laser and electron beams in the coordinate system x, y, z, presented in Fig. 2, let's introduce modified Stokes parameters.

- $\xi_\perp \in [0:1]$ and $\varphi_\perp \in [0:\pi]$ are the degree of laser linear polarization and its azimuthal angle.
- $\xi_\circlearrowleft \in [-1:1]$ is the sign and degree of circular polarization of laser radiation: $\sqrt{\xi_\perp^2 + \xi_\circlearrowleft^2} = 1$.
- $\zeta_\perp \in [0:1]$ and $\phi_\perp \in [0:2\pi]$ are the degree of transverse e± beam polarization and its azimuthal angle.
- $\zeta_\circlearrowleft \in [-1:1]$ is the sign and degree of longitudinal spin polarization of the electrons: $\sqrt{\zeta_\perp^2 + \zeta_\circlearrowleft^2} \in [0:1]$.

Then, the ICS cross section is described by the sum of three terms: $d\sigma = d\sigma_0 + d\sigma_\parallel + d\sigma_\perp$. These terms are: $d\sigma_0$ – unpolarized electron; $d\sigma_\parallel$ – longitudinal electron polarization; $d\sigma_\perp$ – transverse electron polarization:

$$\begin{aligned}
\frac{d\sigma_0}{du\,d\varphi} &= \frac{r_e^2}{\kappa^2(1+u)^3}\Big(\kappa(1+(1+u)^2) - \\
&\quad - 4\frac{u}{\kappa}(1+u)(\kappa-u)\Big[1 - \xi_\perp\cos\big(2(\varphi-\varphi_\perp)\big)\Big]\Big), \\
\frac{d\sigma_\parallel}{du\,d\varphi} &= \frac{\xi_\circlearrowleft\zeta_\circlearrowleft r_e^2}{\kappa^2(1+u)^3}\,u(u+2)(\kappa-2u), \\
\frac{d\sigma_\perp}{du\,d\varphi} &= \frac{-\xi_\circlearrowleft\zeta_\perp r_e^2}{\kappa^2(1+u)^3}\,2u\sqrt{u(\kappa-u)}\cos(\varphi-\phi_\perp).
\end{aligned} \tag{6}$$

In Eq. (6) r_e is the classical electron radius and φ is the observer's azimuthal angle. As one can see from Eq. (6), the last term $d\sigma_\perp$, most important for FCC-ee polarimeter, can not modify the total cross section, which in absence of longitudinal polarization of electrons is obtained by integration of $d\sigma_0$ only:

$$\begin{aligned}
\sigma_0(\kappa) = \frac{2\pi r_e^2}{\kappa}\Bigg[&\left(1 - \frac{4}{\kappa} - \frac{8}{\kappa^2}\right)\log(1+\kappa) + \\
&+ \frac{1}{2}\left(1 - \frac{1}{(1+\kappa)^2}\right) + \frac{8}{\kappa}\Bigg].
\end{aligned} \tag{7}$$

In case when $\kappa \ll 1$ Eq. (7) tends to Thomson cross section $\sigma_0 = \frac{8}{3}\pi r_e^2(1-\kappa)$.

The above expressions are enough e. g. to start Monte-Carlo generator and allow further analysis of scattered particles distributions. The probability distribution of u is defined by the cross section Eq. (6). Then the required properties, like ω, ε, θ_e or θ_γ are obtained using Eq. (1) and Eq. (5). However, the influence of bending magnet in Fig. 2 on scattered electrons is not yet considered.

Bending of Electrons

Let's describe the dipole strength by the parameter B, assuming for the sake of brevity that it is proportional to the integral of magnetic field along the electron trajectory. The electron with energy ε will be bent to the angle $\theta = B/\varepsilon$ under the assumption that B is the same for all energies under consideration [2]. By Eq. (1) we express the energy ε of scattered electron through the ICS parameter u: $\varepsilon = \varepsilon_0/(1+u)$. This electron is bent by the dipole to the angle

$$\theta = \frac{B}{\varepsilon} = \frac{B}{\varepsilon_0} + u\frac{B}{\varepsilon_0} = \theta_0 + u\theta_0, \tag{8}$$

i. e. θ is the sum of the beam bending angle θ_0 and the bending angle $\Delta\theta = u\theta_0$, caused by electron energy loss in ICS. Both θ_0 and $\Delta\theta$ are shown in Fig. 2 for the maximum possible u value $u = \kappa$. Note that $\kappa\theta_0$ does not depend on ε_0 as well as $\max(\theta_e)$. In ref. [8] it was suggested to use the ratio $\Delta\theta/\theta_0 = \kappa$ for beam energy determination at ILC.

Let us introduce a new designation $\vartheta_x \equiv \gamma(\theta - \theta_0) = u\vartheta_0$ which is the angle $\Delta\theta$, measured in units of $1/\gamma$. The electron scattering angle in ICS, expressed in the same units, is $\vartheta = u\sqrt{\kappa/u - 1}$ as it follows from Eq. (5). Combining bending and scattering angles and splitting ϑ into x and y components we get:

$$\begin{aligned}
\vartheta_x &= \sqrt{u(\kappa-u)}\cos\varphi + u\vartheta_0, \\
\vartheta_y &= \sqrt{u(\kappa-u)}\sin\varphi.
\end{aligned} \tag{9}$$

Since backscattered photons are not bent by the dipole, the photon transverse angles (Eq. (5)) in the same space and in the same units, according to similar considerations, are the following:

$$\begin{aligned}
\eta_x &= -\sqrt{\kappa/u - 1}\cos\varphi - \vartheta_0, \\
\eta_y &= -\sqrt{\kappa/u - 1}\sin\varphi.
\end{aligned} \tag{10}$$

[2] The validity of this assumption will be discussed on page 3.

ISBN: 978-3-95450-216-5 doi:10.18429/JACoW-eeFACT2018-TUPBB03

POLARIMETER

The polarimeter will be installed in the FCC-ee section shown in Fig. 3. After the dispersion suppressing dipole magnet, about 100 m of free beam propagation without multipole magnets is reserved for separation of the ICS photons and electrons from the beam. The interaction of the pulsed

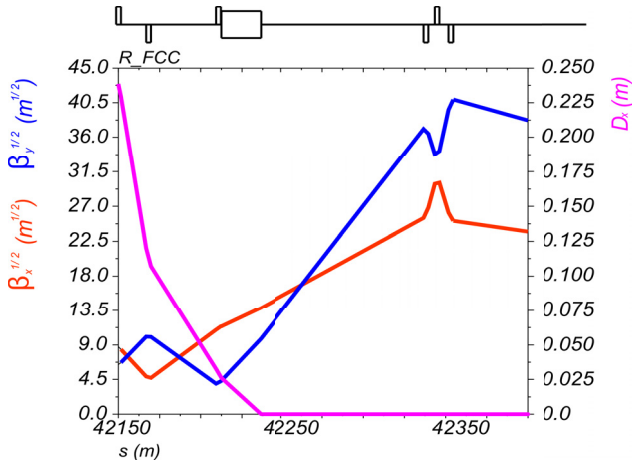

Figure 3: Polarimeter location with respect to FCC-ee lattice.

laser beam with the electron beam occurs just between the dipole and preceding quadrupole, where there is a local minimum of vertical β-function. In Fig. 4 there is the sketch of the polarimeter apparatus arrangement in horizontal plane.

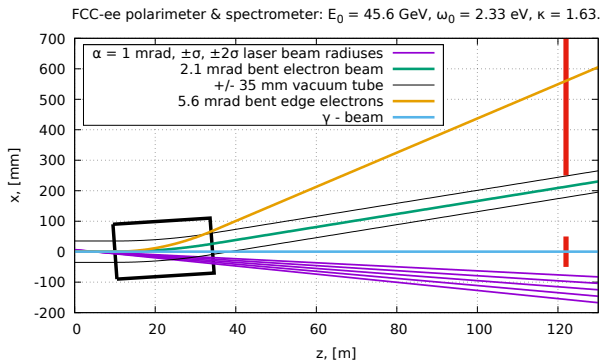

Figure 4: Sketch of the polarimeter: dipole (L = 24.12 m, θ_0 = 2.13 mrad, B = 0.0135 T, R_0 = 11302 m), vacuum chamber, particle trajectories. Red vertical bars on the right side show the location of the scattered particles detectors – 100 m away from the center of the dipole.

The laser radiation λ_0 = 532 nm is inserted to the vacuum chamber from the right and focused to the interaction point (z=5 m). The laser spot transverse size at i. p. is σ_0 = 0.25 mm. According to Fig. 4, laser-electron interaction angle is $\alpha = \pi - 0.001$ and the relative difference between κ from Eq. (2) and $\kappa(\alpha)$ from Eq. (3) is as small as $2.5 \cdot 10^{-7}$.

Spectrometer

Figure 4 helps to understand how much could be the difference of the B-field integral, seen by the electrons with different energies. All of the electrons enter the dipole of length L along the same line – the beam orbit. Then, the radius of trajectory will be dependent on the electron energy. Let R_0 to be the radius of an electron with energy ε_0 and $\theta_0 = L/R_0$ is the beam bending angle. The minimal radius of an electron after scattering on the laser light will be $R_0/(1+\kappa)$. After passing the dipole these two electrons will have the difference $\Delta x \simeq \kappa L\theta_0/2$ in transverse horizontal coordinates. With the parameters of Fig. 4 this difference is $\Delta x \simeq 43$ mm. The length of the trajectories of these two electrons inside the dipole will be also different, i. e. even in case of absolutely uniform dipole their field integrals will not be the same. With rectangular pole shape exact expression for relative difference of the lengths of trajectories is:

$$\frac{\Delta L}{L} = \frac{1}{1+\kappa}\frac{2}{\theta_0}\arcsin\left(\frac{\theta_0}{2}(1+\kappa)\sqrt{1+\left(\frac{\kappa\theta_0}{2}\right)^2}\right) - \\ -\frac{2}{\theta_0}\arcsin\left(\frac{\theta_0}{2}\right). \quad (11)$$

As we see this relative difference depends on θ_0 and κ only. With the set of parameters taken from Fig. 4, i. e. θ_0 = 2.13 mrad and κ = 1.63, $\Delta L/L = 2.63 \cdot 10^{-6}$.

The result of this section is the proof of the validity of assumption about the equality of the integrals of the magnetic field for the electron beam and scattered electrons. This assumption was found to be rather accurate for the dipole with perfectly uniform field, however *shorter dipole is much more preferable* in order to decrease Δx and hence have less concerns about the field quality.

Scattered Photons & Electrons

The Monte-Carlo generator was created to obtain the 2D (x, y) distributions of scattered photons and electrons at the detectors, located as it was shown in Fig. 4. The ICS parameters are: ε_0 = 45.6 GeV and ω_0 = 2.33 eV. The spectrometer configuration is described by the beam bending angle θ_0 = 2.134 mrad, the lengths of the dipole L = 24.12 m and two spectrometer arms. First arm L_1 = 117 m is the distance between laser-electron IP and the detector. Second arm L_2 = 100 m is the distance between the longitudinal center of the dipole and the detector.

The impact of the electron beam parameters is accounted by introducing the angular spreads according to the beam emittances ϵ_x = 0.27 nm and ϵ_y = 1 pm. The horizontal and vertical electron angles x' and y' in the beam are described by normal distributions standard deviations $\sigma_x = \sqrt{\epsilon_x/\beta_x}$ and $\sigma_y = \sqrt{\epsilon_y/\beta_y}$. The generator is arranged as follows:

- raffle $u \in [0, \kappa]$ and $\varphi \in [0 : 2\pi]$ according to 2D function $d\sigma(u, \varphi)$ Eq. (6)),
- raffle x' and y' according to corresponding normal distributions,
- obtain photon X_γ, Y_γ and electron X_e, Y_e transverse coordinates at the detection plane:

ISBN: 978-3-95450-216-5 doi:10.18429/JACoW-eeFACT2018-TUPBB03

$$
\begin{aligned}
X_\gamma &= x' L_1 - \frac{L_1}{\gamma}\sqrt{\kappa/u - 1}\cos\varphi - \theta_0 L_2,\\
Y_\gamma &= y' L_1 - \frac{L_1}{\gamma}\sqrt{\kappa/u - 1}\sin\varphi,\\
X_e &= x' L_1 + \frac{L_1}{\gamma}\sqrt{u(\kappa - u)}\cos\varphi + u\theta_0 L_2,\\
Y_e &= y' L_1 + \frac{L_1}{\gamma}\sqrt{u(\kappa - u)}\sin\varphi.
\end{aligned}
\tag{12}
$$

The results of such a simulation for an electron beam with $\zeta_\perp = 25\%$ vertical ($\phi_\perp = \pi/2$) spin polarization are presented in Fig. 5 and Fig. 6. The difference between the figures is the laser polarization $\xi_\cup = +1$ (Fig. 5) and $\xi_\cup = -1$ (Fig. 6). The 2D distributions for both photons and electrons are plotted along the same horizontal axis x, where $x = 0$ corresponds to the position of the electron beam. The detectors for scattered particles are located outside the machine vacuum chamber. The scattered electrons distribution starts from $x = 40$ mm: this is the radius of the vacuum chamber.

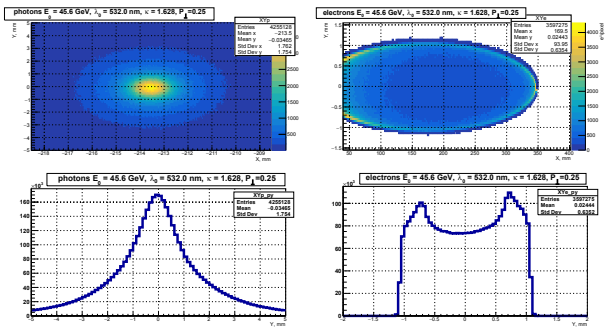

Figure 5: MC results, $P_\perp = \xi_\cup \zeta_\perp = 0.25$ and $\phi_\perp = \pi/2$.

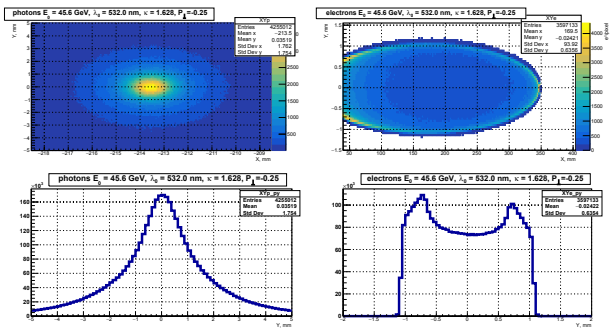

Figure 6: MC results, $P_\perp = \xi_\cup \zeta_\perp = -0.25$ and $\phi_\perp = \pi/2$.

The 1D distributions in the bottom of each figure are the projections of 2D distributions to the vertical axis y. The mean y-values of these distributions are shifted up or down from zero according to the presence of beam polarization and corresponding asymmetries in ICS cross section. In Fig. 7 all distributions are obtained by subtraction of corresponding distributions from Fig. 5 and Fig. 6. Detecting the up-down asymmetry in the distribution of laser backscattered photons is a classical way to measure the transverse polarization of the electron beam. In [9] it was proposed to use the up-down asymmetry in the distribution of scattered electrons for the

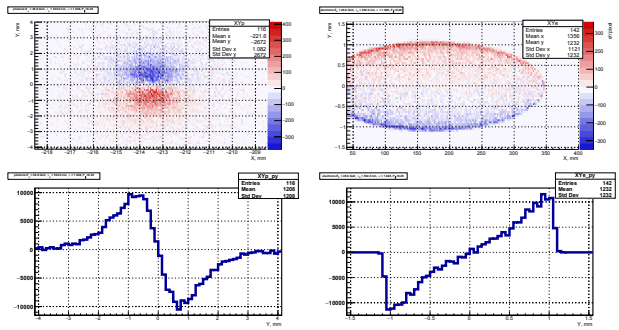

Figure 7: The difference between corresponding distributions in Fig. 5 and Fig. 6.

transverse polarization measurement at the ILC. It was suggested to measure the distribution of scattered electrons by silicon pixel detector.

Maximum up-down asymmetry in the distribution of scattered electrons occurs at the scattering angles of $\theta_e^* = \pm 2\omega_0/mc^2$, which is approximately ± 9 μrad (see Eq. (5) and Eq. (6)). Asymmetry can be observed only if the distribution is not blurred by the electron beam emittance. On the other hand, maximum up-down asymmetry in the distribution of scattered photons occurs at the scattering angles of $\theta_\gamma^* \simeq 1/\gamma$ which is almost the same as θ_e^* in our particular case. But e. g. when beam energy is about 5 GeV, θ_γ^* is ten times larger then θ_e^* and the measurement of beam polarization by photons looks like more preferable. What are the benefits of scattered electrons against scattered photons for the FCC-ee polarimeter?

- Scattered electrons propagate to the inner side of the beam orbit, i. e. there is no direct background from high energy synchrotron radiation.
- Unlike photons, charged electrons are ready to be detected by ionization losses. The photons need to be converted to e^+e^- pairs: this leads either to low detection efficiency either to decrease in spatial resolution.
- Despite the fact that the fluxes of scattered photons and electrons are the same, the flux density of electrons is much lower due to bending and corresponding spatial separation by energies. Simultaneous detection of multiple scattered electrons thus is much easier.
- Analysis of the scattered electrons distribution allows to measure the longitudinal beam polarization as well as the transverse one.
- As one can observe from Figs. 5–7, change of laser circular polarization leads to a redistribution of the scattered electron density within a fixed elliptic shape of distribution. This fact potentially provides better systematic accuracy for beam polarization determination.

Nevertheless both photon and electron distributions are going to be measured by the polarimeter. First, to exploit

ISBN: 978-3-95450-216-5 doi:10.18429/JACoW-eeFACT2018-TUPBB03

directly the LEP and HERA experience. Second, to be able to measure the center of the photon distribution in both x and y dimensions. The latter is required for direct beam energy determination, which will be discussed below.

SCATTERED ELECTRONS

This section owes its origin to the successful application of the method of direct electron beam energy determination by backscattering of laser radiation. The approach is based on the measurement of ω_{max} (see Eq. 4) in cases when this energy can be measured with good accuracy and in absolute scale. For the last years, the positive experience with this approach was accumulated at the low energy colliders VEPP-4M, BEPC-II and VEPP-2000 [10]. Despite the fact that this method is not directly applicable in FCC-ee case, let us try to figure out what can be learned from the elliptical shape of the distribution of scattered electrons, obtained by MC simulations above.

We return to the consideration of the spatial distribution of the scattered electrons. From Eq. (9) we obtain the square equation on u:

$$(\vartheta_x - u\vartheta_0)^2 + \vartheta_y^2 = u(\kappa - u), \tag{13}$$

with the roots $u^{\pm} =$

$$\frac{\kappa + 2\vartheta_0\vartheta_x \pm \sqrt{\kappa^2 - 4(\vartheta_x^2 + \vartheta_y^2(1+\vartheta_0^2) - \kappa\vartheta_0\vartheta_x)}}{2(1+\vartheta_0^2)}. \tag{14}$$

The average value of u and its limiting value for the large values of ϑ_0 do not depend on ϑ_y:

$$\langle u \rangle = \frac{u^+ + u^-}{2} = \frac{\kappa/2 + \vartheta_0\vartheta_x}{1+\vartheta_0^2} \xrightarrow{\vartheta_0 \gg 1} \frac{\vartheta_x}{\vartheta_0}. \tag{15}$$

In the ϑ_x, ϑ_y plane all the scattered electrons are located inside the ellipse (what we have seen in Figs. 5, 6), described by the radicand in Eq. (14). The center of the ellipse is located at the point $[\vartheta_x = \kappa\vartheta_0/2; \vartheta_y = 0]$, its horizontal semiaxis is $A = \kappa\sqrt{1+\vartheta_0^2}/2$ while the verical (along ϑ_y) is $B = \kappa/2$. In particular, this means that

$$\vartheta_x^{max} = \frac{\kappa}{2}\left(\vartheta_0 + \sqrt{1+\vartheta_0^2}\right) \xrightarrow{\vartheta_0 \gg 1} \kappa\vartheta_0. \tag{16}$$

Recall that according to notation introduced above, ϑ-s are the angles measured in units of $1/\gamma$, while θ-s are the angles in radians. In radians expression Eq. (16) looks like

$$\Delta\theta = \frac{\kappa}{2}\left(\theta_0 + \sqrt{1/\gamma^2 + \theta_0^2}\right) \xrightarrow{\theta_0 \gg 1/\gamma} \kappa\theta_0, \tag{17}$$

where $\Delta\theta$ and θ_0 were presented in Fig. 2. In order to rewrite the ICS cross section (Eq. 6) in ϑ_x, ϑ_y variables we calculate the Jacobian matrix $\mathbf{J} = \partial(\vartheta_x, \vartheta_y)/\partial(u, \varphi)$:

$$\mathbf{J} = \begin{bmatrix} \vartheta_0 + \dfrac{\kappa/2 - u}{\sqrt{u(\kappa-u)}}\cos\varphi & -\sqrt{u(\kappa-u)}\sin\varphi \\ \dfrac{\kappa/2 - u}{\sqrt{u(\kappa-u)}}\sin\varphi & \sqrt{u(\kappa-u)}\cos\varphi \end{bmatrix}. \tag{18}$$

The determinant of $\mathbf{J}$ is:

$$\begin{aligned} \det(\mathbf{J}) &= \kappa/2 - u + \vartheta_0\sqrt{u(\kappa-u)}\cos\varphi = \\ &= \sqrt{\kappa^2/4 - \vartheta_x^2 - \vartheta_y^2(1+\vartheta_0^2) + \kappa\vartheta_0\vartheta_x}. \end{aligned} \tag{19}$$

Hence $dud\varphi = 2d\vartheta_x d\vartheta_y/\det(\mathbf{J})$, where "2" is due to the sum of "up" and "down" solutions of Eq. (14). Let us perform another change of variables: instead of ϑ_x, ϑ_y we introduce x and y. With these new variables the cross section exists inside the circle of radius $R = 1$ centered at $(x = 0; y = 0)$:

$$x = \frac{2\vartheta_x/\kappa - \vartheta_0}{\sqrt{1+\vartheta_0^2}}, \qquad y = \frac{\vartheta_y}{\kappa/2}. \tag{20}$$

Then:

$$\begin{aligned} dud\varphi &= \frac{\kappa\, dx\, dy}{\sqrt{1-x^2-y^2}}, \\ u = \langle u \rangle &= \frac{\kappa}{2}\left(1 + \frac{x\vartheta_0}{\sqrt{1+\vartheta_0^2}}\right), \\ \sin(\varphi) &= \frac{y\,\kappa}{2\sqrt{u(\kappa-u)}}. \end{aligned} \tag{21}$$

In Eq. (21) the vertical transverse electron polarization ($\phi_\perp = \pi/2$) is assumed, then $\cos(\varphi - \phi_\perp) = \sin(\varphi)$. Considering backscattering of circularly polarized laser radiation ($\xi_\circlearrowleft = \pm 1$) on the electron beam, where both vertical transverse ($\zeta_\perp \neq 0, \phi_\perp = \pi/2$) and longitudinal ($\zeta_\circlearrowleft \neq 0$) polarizations are possible, we rewrite the cross sections Eq. (6):

$$\begin{aligned} \frac{1}{r_e^2}\frac{d\sigma_0}{dx\,dy} &= \frac{1 + (1+u)^2 - 4(u/\kappa)(1+u)(1-u/\kappa)}{\kappa(1+u)^3\sqrt{1-x^2-y^2}}, \\ \frac{1}{r_e^2}\frac{d\sigma_\parallel}{dx\,dy} &= \xi_\circlearrowleft\zeta_\circlearrowleft\frac{u(u+2)(1-2u/\kappa)}{\kappa(1+u)^3\sqrt{1-x^2-y^2}}, \\ \frac{1}{r_e^2}\frac{d\sigma_\perp}{dx\,dy} &= -\xi_\circlearrowleft\zeta_\perp\frac{uy}{\kappa(1+u)^3\sqrt{1-x^2-y^2}}. \end{aligned} \tag{22}$$

Due to the term $\sqrt{1-x^2-y^2}$ in the denominator of Eq. (22) the cross section has singularity a the edge of a circle (ellipse), which however is integrable.

Fitting the Distribution

The detectors for scattered photons and electrons are going to be installed as it was shown in Fig 4. For the detection of scattered electrons we consider a position measurement using a silicon pixel detector (as in [9]) placed at the distance $L_1 = 117$ m from the Compton IP and $L_2 = 100$ m from the center of bending dipole. The active dimension of the detector is 400×4 mm^2, it is shifted horizontally 40 mm away from the beam axis, assuming the given size of vacuum chamber. The size of the pixel cell taken is 2×0.05 mm^2, i. e. there are 200 pixels in x and 80 pixels in y.

The pixel detectors for photons (with thin converter) and electrons will measure the x and y positions of each particle according to the scheme shown in Fig 8.

ISBN: 978-3-95450-216-5 doi:10.18429/JACoW-eeFACT2018-TUPBB03

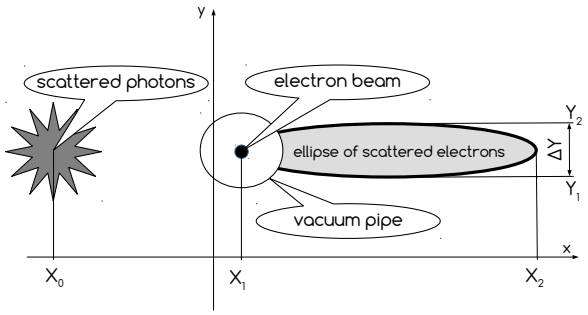

Figure 8: The xy plane of particle detection. X_0 is the horizontal center of gravity in the scattered photons distribution. X_1 is the electron beam position and at the same time – the left edge of the scattered electrons ellipse, while X_2 is the right side of the ellipse. Vertical size $\Delta Y = L_1 \cdot (4\omega_0/mc^2)$.

We will fit the MC distribution of scattered electrons by theoretical cross section Eq. (22). This cross section has a very sharp edge at $x^2 + y^2 = 1$ so the integrals of Eq. (22) over each pixel are required for fitting. The cross section dependencies on u and y are much smoother so it was found to be enough to take the integral

$$I_{xy} = \int_{x_0}^{x_1} \int_{y_0}^{y_1} \frac{dx\,dy}{\sqrt{1-x^2-y^2}} \tag{23}$$

over a rectangular pixel limited by $[x_0, x_1]$ in x and $[y_0, y_1]$ in y which is not difficult to do analytically.

The second step is to calculate the convolution of I_{xy} with the two-dimensional normal distribution of initial electrons: $P(x,y) = \frac{1}{2\pi\sigma_x\sigma_y} \exp\left(-\frac{x^2}{2\sigma_x^2} - \frac{y^2}{2\sigma_y^2}\right)$. It is not hard to show, that σ_x and σ_y are the RMS electron beam sizes (due to betatron and synchrotron motion) at the plane of detection. The last step is to account for the cross section dependencies on u and y parameters in Eq. (22).

The $F(x,y)$ function was built based on these considerations in order to describe the shape of the scattered electrons distribution, see Fig. 9. It has nine parameters except normalization:

- The first parameter is κ, defined in Eq. (2). This parameter is fixed according to approximate value of the beam energy cause $F(x,y)$ weakly depends on κ, ±1% changes does not matter on the fit results.
- The next four parameters are X_1, X_2, Y_1, Y_2 – positions of the ellipse edge, see Fig. 8.
- The sixth and seventh are responsible for polarization sensitive terms $P_\perp = \xi_\cup \zeta_\perp$ and $P_\parallel = \xi_\cup \zeta_\cup$. In the example below the fixed conditions are $\phi_\perp = \pi/2$ and $\zeta_\cup = 0$.
- The eighth and ninth are σ_x and σ_y – the electron beam sizes at the azimuth of the detector.

Fig. 9 shows the results of numerical experiment with the initial parameters $\varepsilon_0 = 45.6\,\text{GeV}$, $\lambda_0 = 532\,\text{nm}$, $P_\perp = 0.1$ and $2 \cdot 10^7$ scattering events. The distribution of scattered electrons was then fitted by the function $F(x,y)$.

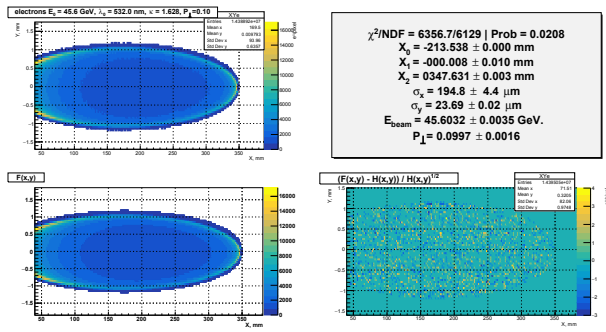

Figure 9: *Top-left:* MC distribution of scattered electrons $H(x,y)$. *Bottom-left:* function $F(x,y)$ after fitting. *Bottom-right:* normalized difference: $(F(x,y) - H(x,y))/\sqrt{H(x,y)}$. *Top-right:* the $F(x,y)$ parameters obtained by fitting (except X_0, which is the mean x value of the photons distribution).

The parameters obtained directly from the fit are the ellipse edge positions X_1, X_2, Y_1, Y_2, beam transverse sizes σ_x and σ_y and the beam polarization degree $P_\perp$. In this experiment $P_\perp$ is measured with 1.6% accuracy (0.16% absolute accuracy). The beam energy, E_{beam} in Fig. 9, and its measurement accuracy (≃ 80 ppm) were evaluated from X_0, X_1 and X_2:

$$E_{beam} = \frac{(mc^2)^2}{4\omega_0} \cdot \frac{X_2 - X_1}{X_1 - X_0}. \tag{24}$$

SCATTERING RATE

Consider CW TEM_{00} laser radiation propagating along z-axis. If laser light of wavelength λ_0 is focused at $z = 0$ to the waist size of σ_0, the beam size will evolve along z:

$$\sigma(z) = \sigma_0 \sqrt{1 + \left(\frac{z}{z_R}\right)^2}, \tag{25}$$

where $z_R = 4\pi\sigma_0^2/\lambda_0$ is the Rayleigh length. The optical intensity [W/cm^2] in a Gaussian beam of power P [W] is:

$$I(r,z) = \frac{P}{2\pi\sigma(z)^2} \exp\left(-\frac{r^2}{2\sigma(z)^2}\right). \tag{26}$$

Far field divergence is $\theta = \sigma_0/z_R = \lambda_0/4\pi\sigma_0$. Laser radiation power is the number of photons emitted per second:

$$P = dE/dt = h\nu \cdot dN/dt \ \ [\text{J s}^{-1}]. \tag{27}$$

Thus the longitudinal density of laser photons along z is: $\rho_\parallel = dN/dz = P\lambda_0/hc^2$ [cm^{-1}]. Consider an electron ($v/c \simeq 1$) propagating towards the laser head sea with small incident angle α as illustrated by Fig. 10. The photon target

ISBN: 978-3-95450-216-5 doi:10.18429/JACoW-eeFACT2018-TUPBB03

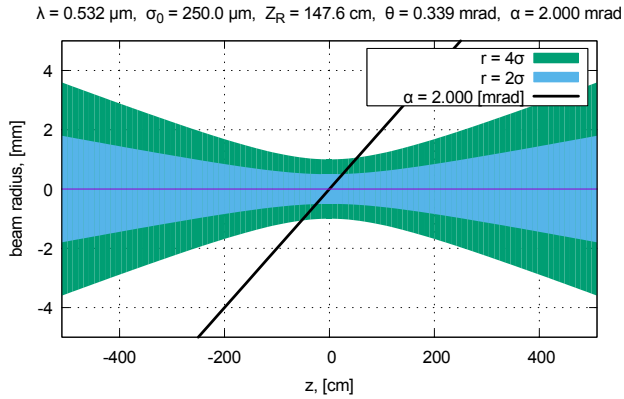

Figure 10: An electron (the black sloping line) passing through the laser beam waist.

density for this electron is defined as:

$$\rho_\perp = \rho_\parallel \frac{(1+\cos\alpha)}{2\pi\sigma_0^2} \int_{-\infty}^{\infty} \frac{\exp\left(-\frac{z^2\tan^2\alpha}{2\sigma(z)^2}\right)}{1+(z/z_R)^2} dz \ \ [\mathrm{cm}^{-2}]. \quad (28)$$

Scattering probability W is determined by the product of $\rho_\perp$ and the scattering cross section. The latter is defined by Eq. (7) and depends on κ parameter, see Fig. 11.

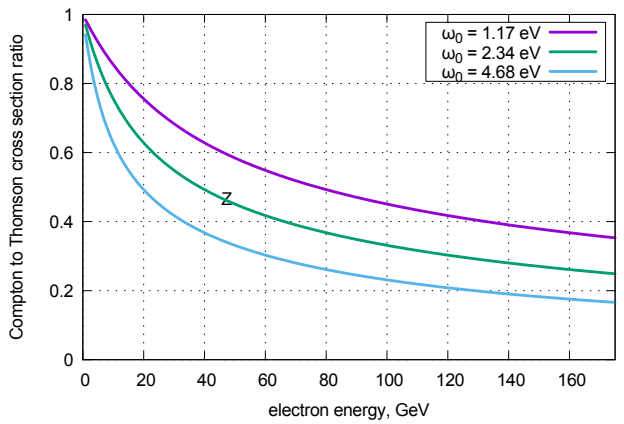

Figure 11: The ratio of the ICS cross section to Thomson cross section vs electron energy.

Maximum scattering probability W_{max} is reached in case $\alpha = 0$ and at low energy with Thomson cross section $\sigma_T = 0.665$ barn.

$$W_{max} = \frac{\sigma_T}{\pi\sigma_0^2}\frac{P\lambda_0}{hc^2}\int_{-\infty}^{\infty}\frac{dz}{1+(z/z_R)^2} = \frac{4\pi\sigma_T P}{hc^2} = \frac{P}{P_c}, \quad (29)$$

where $P_c = \hbar c^2/2\sigma_T \simeq 0.7124\cdot 10^{11}$ [W] is the power of laser radiation required for 100% scattering probability. We see that W_{max} depends neither on the radiation wavelength λ_0 nor the waist size σ_0, but on the laser power only. A low energy electron bunch with $0.7\cdot 10^{11}$ population colliding head-on with 1 W of laser radiation will produce one Compton scattering event – this is true if the transverse sizes of the electron bunch is much smaller then the laser ones.

The loss in scattering probability when $\alpha \neq 0$ is defined by the ratio of angle α to the laser divergence angle $\theta = \sigma_0/z_R$. Since the mirror is required in order to deliver the laser beam to IP, θ should be always smaller than α: this ratio finely will describe the laser and electron beam separation at the place of mirror installation (see Fig. 4). If we define the "Ratio of Angles" as $R_A = \alpha/\theta$, probability loss will be expressed as:

$$\eta(R_A) = \frac{W(\alpha)}{W_{max}} = \frac{1}{\pi}\int_{-\infty}^{\infty}\exp\left(-\frac{x^2R_A^2}{2(1+x^2)}\right)\frac{dx}{1+x^2}. \quad (30)$$

The result of numerical integration is presented in Fig. 12.

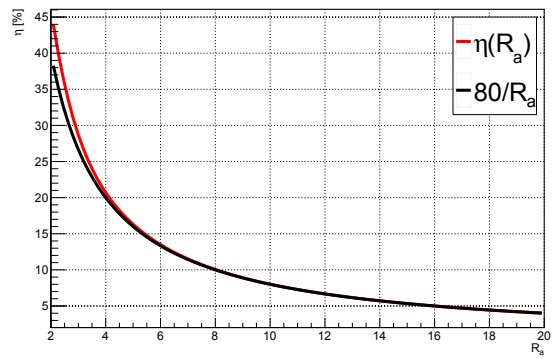

Figure 12: $\eta(R_A)$ vs R_A by Eq. (30) and its approximation.

At the FCC-ee there will be polarized pilot bunches for regular beam energy measurement by resonant depolarization. So the laser system should provide the backscattering on a certain electron bunch: the laser operation in CW mode is thus not possible. The FCC-ee revolution frequency $\simeq$ 3 kHz is comfortable for solid-state lasers operating in a Q-switched regime. The laser pulse propagation can be described as:

$$\rho_\parallel(s,t) = \frac{N_\gamma}{\sqrt{2\pi}c\tau_L}\exp\left(-\frac{1}{2}\left(\frac{s-ct}{c\tau_L}\right)^2\right), \quad (31)$$

where τ_L and E_L are pulse duration and energy, $N_\gamma = E_L\lambda/hc$. Scattering probability for $\alpha = 0$ is:

$$W = \frac{P_L}{P_c}\cdot\int_{-\infty}^{\infty}\frac{\exp\{-2(xR_L)^2\}}{\pi(1+x^2)}dx, \quad (32)$$

where $P_L = E_L/\sqrt{2\pi}\tau_L$ is the instantaneous laser power and $R_L = z_R/c\tau_L$ is the "Ratio of Lengths". The scattering probability for an arbitrary α is:

$$W = \frac{P_L}{P_c}\cdot\eta(R_L,R_A), \text{ where}$$
$$\eta(R_L,R_A) = \int_{-\infty}^{\infty}\frac{\exp\left(-x^2\left(2R_L^2+\frac{R_A^2}{2(1+x^2)}\right)\right)}{\pi(1+x^2)}dx. \quad (33)$$

ISBN: 978-3-95450-216-5 doi:10.18429/JACoW-eeFACT2018-TUPBB03

The map of the efficiency $\eta(R_L, R_A)$, obtained by numerical integration of Eq. (33), is presented in Fig. 13.

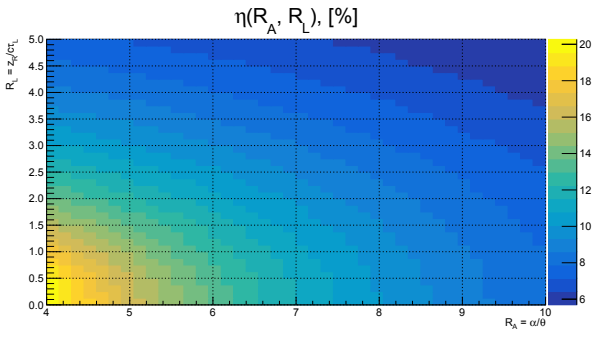

Figure 13: $\eta(R_L, R_A)$ color map.

Now we have enough instruments to estimate the flux of backscattered photons, obtained from one FCC-ee bunch in the configuration, shown in Fig. 4.

- Beam electron energy $E_{beam} = 45.6\,\text{GeV}$.
- Laser wavelength $\lambda_0 = 532\,\text{nm}$.
- Cross section (letter Z on Fig. 11): $R_\times \simeq 50\%$.
- Waist size $\sigma_0 = 0.25\,\text{mm}$, $z_R = 148\,\text{cm}$.
- Far field divergence $\theta = 0.169\,\text{mrad}$.
- Interaction angle $\alpha = 1.0\,\text{mrad}$ (horizontal crossing).
- Laser pulse: $E_L = 1$ [mJ], τ_L=5 ns, $f = 3\,\text{kHz}$.
- Instantaneous power: $P_L = 80\,\text{kW}$, $P_L/P_c = 1.1 \cdot 10^{-6}$.
- Ratio of angles $R_A = 5.9$, ratio of lengths $R_L = 0.98$.
- $\eta(R_L, R_A) \simeq 13\%$ (see Fig. 13).
- Scat. probability $W = P_L/P_c \cdot R_\times \cdot \eta(R_L, R_A) \simeq 7 \cdot 10^{-8}$.
- $N_e = 10^{10}$ e±/bunch: $\dot{N}_\gamma = f \cdot N_e \cdot W \simeq 2 \cdot 10^6$ [s^{-1}].
- Average laser power is $P = f \cdot E_L \simeq 3$ W.

The influence of the electron beam sizes on the above estimations was not considered cause here it is nonessential.

SUMMARY

The electron beam polarimeter for the FCC-ee project has been considered. With the laser system parameters, described in the latter section, it allows to measure transverse beam polarization with required 1% accuracy every second. With the suggested scheme, this apparatus can also measure the beam energy, longitudinal beam polarization, beam position and transverse beam sizes at the place of installation. The statistical accuracy of direct beam energy determination is $\Delta E/E < 100$ ppm within 10 s measurement time. The possible sources of systematical errors require additional studies. The best case of such studies would be the experimental test of the suggested approach on low-emittance and low-energy electron beam.

REFERENCES

[1] M. Placidi and R. Rossmanith, "e+ e- polarimetry at LEP", *Nucl. Instrum. Meth.*, A274:79, 1989.

[2] L. Knudsen, J.P. Koutchouk, M. Placidi, R. Schmidt, M. Crozon, J. Badier, A. Blondel, and B. Dehning, "First observation of transverse beam polarization in LEP", *Physics Letters B*, 270(1):97–104, nov 1991.

[3] D.P. Barber, H.-D. Bremer, M. Böge, R. Brinkmann, W. Brückner, Ch. Büscher, M. Chapman, K. Coulter, P.P.J. Delheij, M. Düren, E. Gianfelice-Wendt, P.E.W. Green, H.G. Gaul, H. Gressmann, O. Häusser, R. Henderson, T. Janke, H. Kaiser, R. Kaiser, P. Kitching, R. Klanner, P. Levy, H.-Ch. Lewin, M. Lomperski, W. Lorenzon, L. Losev, R.D. McKeown, N. Meyners, B. Micheel, R. Milner, A. Mücklich, F. Neunreither, W.-D. Nowak, P.M. Patel, K. Rith, Ch. Scholz, E. Steffens, M. Veltri, M. Vetterli, W. Vogel, W. Wander, D. Westphal, K. Zapfe, and F. Zetsche, "The HERA polarimeter and the first observation of electron spin polarization at HERA", *Nuclear Instruments and Methods in Physics Research Section A: Accelerators, Spectrometers, Detectors and Associated Equipment*, 329(1-2):79–111, may 1993.

[4] M. Woods, "The Scanning Compton polarimeter for the SLD experiment", In *High-energy spin physics. Proc. 12th International Symposium, SPIN 96, Amsterdam, Netherlands, September 10-14, 1996*, pages 843–845, 1996.

[5] Aleksandr N Skrinskii and Yurii M Shatunov, "Precision measurements of masses of elementary particles using storage rings with polarized beams", *Soviet Physics Uspekhi*, 32(6):548–554, 1989.

[6] L. Arnaudon, L. Knudsen, J.P. Koutchouk, R. Olsen, M. Placidi, R. Schmidt, M. Crozon, A. Blondel, R. Aßmann, and B. Dehning, "Measurement of LEP beam energy by resonant spin depolarization", *Physics Letters B*, 284(3-4):431–439, jun 1992.

[7] V.B. Berestetskii, E.M. Lifshitz, and L.P. Pitaevskii. *Quantum Electrodynamics*. Butterworth-Heinemann, 1982. pp. 354-368.

[8] N. Muchnoi, H.J. Schreiber, and M. Viti, "ILC beam energy measurement by means of laser compton backscattering", *Nuclear Instruments and Methods in Physics Research Section A: Accelerators, Spectrometers, Detectors and Associated Equipment*, 607(2):340–366, aug 2009.

[9] Itai Ben Mordechai and Gideon Alexander, "A Transverse Polarimeter for a Linear Collider of 250 GeV e± Beam Energy", In *Helmholtz Alliance Linear Collider Forum: Proc. the Workshops Hamburg, Munich, Hamburg 2010-2012, Germany*, pages 577–590, Hamburg, 2013. DESY.

[10] M. N. Achasov and N. Yu. Muchnoi, "Laser backscattering for beam energy calibration in collider experiments", *JINST*, 12(08):C08007, 2017.